Cobalt addition effects on martensitic transformation and microstructural properties of high-temperature Cu–Al–Fe shape-memory alloys

Koksal Yildiz · Mediha Kök · Fethi Dağdelen

Abstract The effects of the addition of Co on the martensitic transformation and microstructural properties of high-temperature Cu–Al–Fe shape-memory alloy systems were studied by means of DSC, XRD, optical microscopy and Vickers microhardness measurements. DSC analyses indicated that the Cu–Al–Fe alloy displayed high-temperature shape-memory characteristics and that the Co additions dramatically influenced the martensitic transformation of the alloys. Structural and morphological investigations showed that the alloys had 18R martensite structure and contained different precipitates. With increasing amounts of Co, it was seen that elemental compositions of precipitates changed and their volume fractions increased and, therefore, both thermal stability and microhardness values of the alloys were affected. As a result, whereas microhardness values of the alloys were increased by 313 ± 7.76 to 365.75 ± 7.84 Hv, the alloys exhibited poor thermal stability and high volume fraction of precipitates following Co addition.

Keywords Cu–Al–Fe · High-temperature martensite · DSC · Microhardness

Introduction

Thermoelastic martensitic transformation of metals and alloys generally occurs at cryogenic temperatures, around 100 °C and above. The working temperature of the resulting shape-memory alloys is in the range of −100 to 100 °C. In these temperature ranges, they are employed as actuators. However, robotic, automobile, aerospace and aeronautics applications required the development of high-temperature shape-memory alloys that allow conversion at 200–1,000 °C [1–3].

Cu-based and NiTi shape-memory alloys are an important group of alloys used as actuators and sensors in industrial applications owing to their shape-memory effect. The working temperature of these alloys depends on the martensitic transformation temperature. The martensitic transformation temperature of Cu-based and NiTi alloys is 150 °C or below. Because these shape-memory alloys are not suitable for use in high-temperature applications such as rocket fuels and automobile engines, there is the demand for the production of high-temperature shape-memory alloys [4].

Copper-based alloys are notable for their easy production and application in addition to their lower price compared to NiTi alloys. Cu-based alloys are generally produced as double alloy systems such as Cu–Zn, Cu–Al and Cu–Sn. Among these alloys, Cu–Sn does not show good thermoelastic transformation. Furthermore, Cu–Sn alloy has rather limited application due to being brittle. The potential uses and properties are improved by the addition of Al, Si, Sn or G to Cu–Zn alloys and by the addition of Ni, Be, Zn and Mn to Cu–Al alloys [5–7]. In this study, a new high-temperature shape-memory alloy group, Cu-Al-Fe alloy, was investigated. Cu-Al-Fe alloy can be produced inexpensively and is expected to have many uses in the future. The ability of Co to improve the properties of the alloy and the thermal and crystal properties and microstructure of the alloy were investigated.

Experimental

$Cu_{82-x}Al_{13}Fe_5Co_x$ ($x = 0,1,2$, in mass%) alloys were prepared by mixing high-purity Cu, Al, Fe and Co in powder

K. Yildiz (✉) · M. Kök · F. Dağdelen
Department of Physics, Firat University, 23119 Elazig, Turkey
e-mail: kyildiz@firat.edu.tr

form, preparing pellets and melting them in an arc furnace. The procedure in the arc furnace was repeated several times, and the alloy in ingot form was homogenized. The alloy groups were identified as CAF-0 ($Cu_{82}Al_{13}Fe_5$), CAF-1 ($Cu_{81}Al_{13}Fe_5Co_1$) and CAF-2 ($Cu_{80}Al_{13}Fe_5Co_2$) based on their Co content. The alloys were kept in a tube furnace at 900 °C for 24 h to improve homogeneity and cooled instantly in ice brine. Samples cut from the ingot were used in determining the physical characteristics of the produced alloys. The martensitic transformation temperature of the alloy groups was determined by Perkin Elmer Sapphire differential scanning calorimeter (DSC) measurements taken at a heating/cooling rate of 20 °C min^{-1} in N_2 gas atmosphere. Crystal structure analyses were carried out at room temperature using a Bruker Discover D8 X-ray diffractometer (XRD). In order to investigate surface morphologies and microhardness changes of the alloys, optical microscope and Vickers hardness measurements were taken. After polishing of the alloy samples, they were etched in 20 mL HCl, 5 g $FeCl_3$–H_2O and 96 mL methanol. The etched samples were examined by using Nikon Eclipse MA200 optical microscope. Microhardness measurements of the samples were performed via Emco test Durascan testing machine. The chemical compositions of the precipitates in alloys were determined by a scanning electron microscope (SEM, ZEISS EVO 40) equipped with an energy dispersive X-ray spectrometer (EDS).

Results and discussion

The DSC measurements of the CAF-0, CAF-1 and CAF-2 samples (Fig. 1), the calculated mean enthalpy values, the temperature transition region (TTR, A_f–M_f) values and the transformation temperature range (A_f–M_s) are presented in Table 1. The transformation temperature of nearly 300 °C for CAF-0, CAF-1 and CAF-2 indicated that the alloys displayed high-temperature shape-memory characteristics. This result is in accordance with previous reports [8]. Addition of iron into the Cu–Al alloys allowed the transformation to take place at a high temperature. The transformation temperature and the enthalpy value of the high-temperature Cu–Al–Fe shape-memory alloy were both lowered by the addition of Co, whereas the transformation temperature range was wider. Some application (such as pipe joining, deployable space structures, heat engine working) may require very large hysteresis in order to maintain a stable austenite phase with in a large temperature range. These alloys can be used different application [9]. Aydogdu et al. [10] reported that Co addition into CuAl alloys at various percent ratios lowered the transformation temperature and the enthalpy value in the same manner observed in the present study. Co reduces the grain
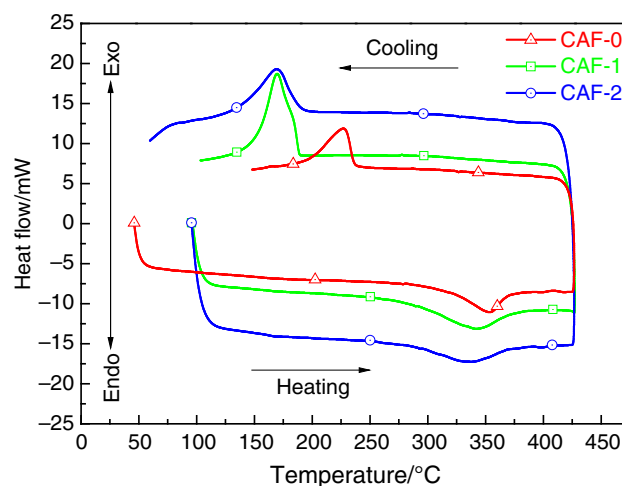

Fig. 1 DSC curves of shape-memory CAF-0, CAF-1 and CAF-2 alloy samples

size of the alloy, thus reducing the transformation temperature [11, 12] and increasing the temperature range.

Optical micrographs showing the surface morphologies of the CAF-0, CAF-1 and CAF-2 samples are presented in Fig. 2a–c, respectively. An initial inspection of the images indicates that all three alloys were clearly in the martensitic phase at room temperature. The microstructure of CAF-0 was coarsely granulated with fine martensitic variants (Fig. 2a). This characteristic morphological structure of the martensitic variants indicates that the dominant martensitic phase of the alloy CAF-0 at room temperature was 18R structured β_1' martensitic phase. A careful investigation of Fig. 2a revealed the absence of γ_1' martensitic variants with a thicker variant morphology, which is proof of the presence of 2H martensitic structures in CAF-0. Figure 2a also shows the presence of tiny sparsely dispersed precipitates with sizes varying in the range of ~1–10 μm within the structure of the alloy CAF-0. The surface morphology of sample CAF-1 is displayed in Fig. 2b. The variants belonging to β_1' martensitic phase were quite distinctive in the microstructure. A comparison of the microstructure of this alloy with that of CAF-0 indicated that the addition of 1 % Co (in mass) partially reduced the grain size. This addition also increased the number and size of precipitates present in the microstructure. The mean size of the precipitates in CAF-1 varied in the range of ~2.5–12 μm as shown in Fig. 2b. The optical micrograph of the CAF-2 alloy sample is shown in Fig. 2c. The substantial decrease in grain size with the further increase of Co content in CAF-2 can be clearly seen in Fig. 2c. The martensitic variants were observed to possess a typical β_1' structure. The numerical distribution and the size of the precipitates in the microstructure were also higher. The mean size of the precipitates varied in the range of ~3.3–14.2 μm. In conclusion, the microstructural variations among the CAF-

Table 1 The transformation temperature parameters of the alloy samples

	A_s/°C	A_f/°C	M_s/°C	M_f/°C	ΔH/Jg/°C	TTR/°C	A_f–M_s/°C
CAF-0	303.8	365.9	236.3	191.7	8.26	174.2	133.2
CAF-1	287.1	369.5	188.4	151.7	7.58	217.8	181.1
CAF-2	275.8	374.9	190.0	133.8	5.83	241.1	185.0
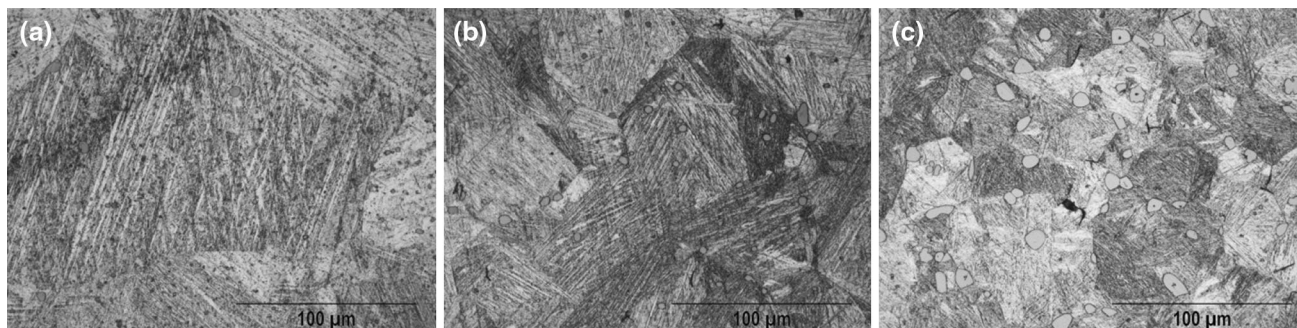
Fig. 2 Optic micrographs showing the surface morphologies of **a** CAF-0, **b** CAF-1 and **c** CAF-2 alloy samples

0, CAF-1 and CAF-2 alloy samples, which were produced using the same methodology, homogenized under similar conditions and possessed the same Al content, is assumed to be directly associated with the differences in the Co content of the samples. The Co atoms dispersed in the matrix possibly had a grain thinning effect on the shape-memory Cu–Al–Fe alloy system given that the grain size was observed to be thinner and smaller with increasing Co content. Kürüm [13] introduced Co in varying concentrations into a Cu–Al alloy system in a previous work and observed metallographically that the grain size of Cu–Al–Co alloy decreased with increasing Co content. Alloying with Co has been previously reported to decrease the grain size of alloys in other studies as well [14]. Gil and Guilemany [15] computed that the grain growth coefficients of shape-memory Cu–Zn–Al alloys decreased upon the addition of Co.
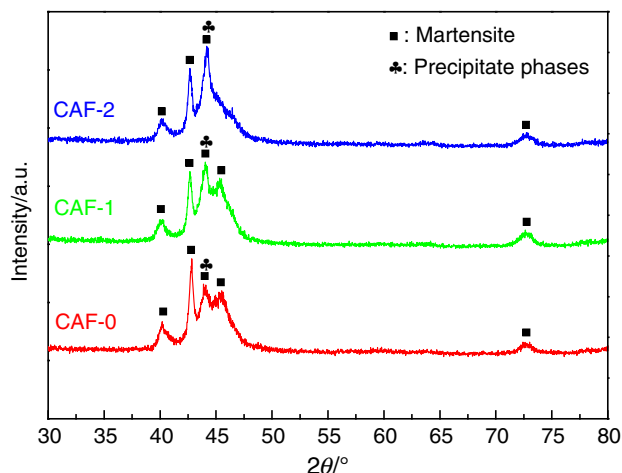
At temperatures below 567 °C, two different phases were observed in binary Cu–Al alloy systems with nearly 13 % (in mass) Al content; the α phase, in which Al solute is in copper solvent and the Cu_9Al_4 phase with the $D8_3$ crystal structure [16, 17]. At the same time, in the ternary Cu–Fe–Al system, two different phase areas may occur due to Cu, Al and Fe contents: $Cu_3Al + Cu_9Al_4$ and Cu_3-Al + FeAl [8, 18]. The presence of the fragile Cu_9Al_4 phase has been reported to cause changes in both the mechanical properties and the thermal stability characteristics of Cu–Al-based shape-memory alloys [19–21]. The chemical compositions of the precipitate phases included in the microstructures of CAF-0, CAF-1 and CAF-2 alloy

samples were identified separately by EDS spectra. The results are shown in Table 2. In Table 2, it can be seen that precipitate phases of CAF-0, CAF-1 and CAF-2 alloy samples have Fe(Al,Cu) and Fe(Al,Cu)–Co compounds, respectively. Yang et al. [8] detected Fe(Al,Cu) phase precipitates in quenched state $Cu_{84}Al_{11}Fe_5$ and $Cu_{83}Al_{12}$-Fe_5 alloys and stated that the precipitate phase related to the Al content and Fe addition will affect both thermal stability and mechanical and shape-memory properties of Cu–Al–Fe shape-memory alloys. This finding is in accordance with what was observed in the DSC curves in Fig. 1 for the alloys CAF-0, CAF-1 and CAF-2 and in the optical microscope images given in Fig. 2; as expected, upon an increase in the relative ratio of the precipitate phases within the alloy, the thermal stability of the alloys was weakened in accordance with the decrease in the enthalpy values of the alloys.

The XRD patterns of the CAF-0, CAF-1 and CAF-2 alloy samples are shown in Fig. 3. The XRD patterns indicated that the crystallographic properties of all three samples were very similar and possessed diffraction peaks belonging to the typical 18R martensitic structure in coherence with morphological observations that were made based on the images displayed in Fig. 2. Interestingly, the intensity of the diffraction peak observed at $2\theta \approx 44°$ in CAF-0 was increased with increasing Co content in the CAF-1 and CAF-2 alloy samples. This peak usually corresponds to the (12–8) diffraction in 18R martensitic structures [22–24], whereas it corresponds to the (110) diffraction in the FeAl structure (Card No:14-0336). For
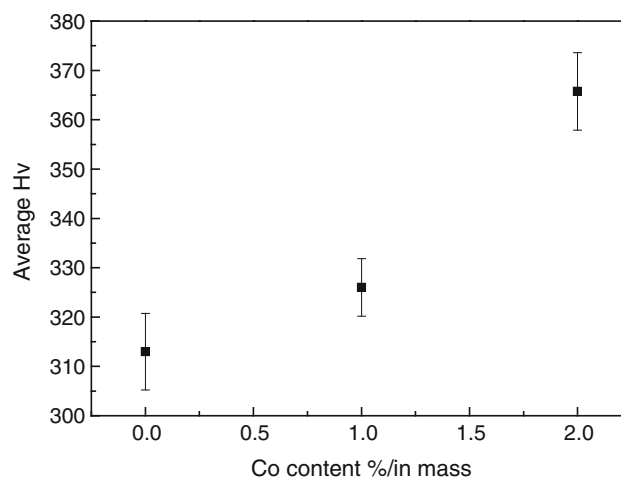
Table 2 EDS results of the precipitates in CAF-0, CAF-1 and CAF-2 alloys

	Cu		Al		Fe		Co	
	Mass%	Atomic%	Mass%	Atomic%	Mass%	Atomic%	Mass%	Atomic%
CAF-0	17.47	13.96	11.31	21.29	71.22	64.76	–	–
CAF-1	21.29	16.07	18.36	32.63	48.60	41.73	11.76	9.57
CAF-2	18.78	13.95	20.23	35.40	40.14	33.94	20.85	16.17

Fig. 3 XRD patterns of CAF-0, CAF-1 and CAF-2 alloy samples

Fig. 4 Variation of average Vickers microhardness values with Co content

CAF-0 alloy samples, when taken together with the results of EDS analysis, the precipitate phase constituting the (110) diffraction line is Fe(Al,Cu) compound. We observed the diffraction peaks for these two phases to overlap, indicating the presence of a direct relationship between the Co content and the intensity of the diffraction peak. The increase in this compound diffraction peak was consistent with the metallographic observations (Fig. 2). It is very well established that an increase in the peak intensity in an XRD pattern can be used as a measure of the increase in the extent of the phase that the peak belongs to. The increasing number of Co atoms in the CAF-1 and CAF-2 alloys in comparison to its absence in CAF-0 caused Co atoms to precipitate from the matrix, resulting in more and larger precipitate structures of the compound Fe(Al,Cu)–Co. Therefore, the increase in the peak intensity of the diffraction of the X-ray at $2\theta \approx 44°$ in the CAF-1 and CAF-2 alloys was likely caused by an increasing amount of the Fe(Al,Cu)–Co phase in these alloys.

The microhardnesses of the CAF-0, CAF-1 and CAF-2 alloy samples were determined by taking Vickers microhardness measurements. Four different measurements from different locations on the sample were performed to determine the overall microhardness value. The average microhardness values for the CAF-0, CAF-1 and CAF-2 alloy samples as a function of the Co content of the samples are plotted in Fig. 4. The plot indicated a considerable increase in the microhardness of the Cu–Al–Fe alloy system upon addition of increasing amounts of Co. The Vickers microhardness value of the alloy CAF-0, which did not have any Co in its structure, was 313 ± 7.76 Hv, whereas this value increased to 326 ± 5.84 and 365.75 ± 7.84 Hv for the CAF-1 and CAF-2 alloys, respectively. The addition of Co increased the microhardness of the Cu–Al–Fe system as expected. Aydogdu et al. [10] added Co to a Cu–Al alloy system in various ratios (0.5–2, in mass%) and observed an increasing trend in the microhardness value of the Cu–Al–Co shape-memory alloy system in the range of 219–295 Hv with increasing Co content. However, we believe that the high microhardness values that the CAF-0, CAF-1 and CAF-2 alloys possessed were not entirely due to the presence of Co. Several values have been reported in the literature for the microhardness values of Cu-based shape-memory alloys: Sari [25] reported the microhardness of Cu–11.9Al–3.8Ni alloy as 230 Hv; Kayali et al. [26] reported the microhardness values for as-quenched Cu–Zn–Al alloys with various compositions as 147 and 196 Hv; and Matlakhova et al. [27] reported the microhardness value for Cu–13.5Al–4Ni alloy as 300.5 ± 20.4 Hv. Therefore, we believe that the formation of the precipitate phases in the microstructure of the

CAF-0, CAF-1 and CAF-2 alloy samples was also causative factor for these high microhardness values.

Conclusions

1. DSC analyses indicated that $Cu_{82-x}Al_{13}Fe_5Co_x$ ($x = 0$, 1, 2 in mass%) alloy samples displayed high-temperature shape-memory characteristics and that both the transformation temperature and the enthalpy values decreased with increasing Co content.
2. Addition of Co affected morphological properties of the Cu–Al–Fe alloy system. The microstructure of CAF-0 alloy that does not include Co consists of 18R martensite structure and Fe(Al,Cu) compound. With the addition of Co, chemical composition of the precipitate phase of CAF-1 and CAF-2 alloys changed to 18R martensite structure and Fe(Al,Cu)–Co compound. With the surplus Co content, the Co content in the precipitate phases of CAF-1 and CAF-2 alloy samples increased. Additionally, surplus Co content caused a decrease in grain size of alloy samples and a significant increase in size and number of precipitate phase.
3. XRD patterns of CAF-0, CAF-1 and CAF-2 alloy samples yielded results consistent with metallographic observations and EDS analyses. It can be seen that phase structure of CAF-0 alloy consists of 18R martensite and Fe(Al,Cu) compounds, while CAF-1 and CAF-2 alloys consist of 18R martensite and Fe(Al,Cu)–Co compounds.
4. The microhardness values of the alloy samples were considerably high since the volume fraction of the precipitate phases in the alloy systems also increased upon Co addition.

References

1. Firstov GS, Van Humbeeck J, Koval YN. High temperature shape memory alloys some recent developments. Mater Sci Eng A. 2014;378:2–10.
2. Padula II S, Bigelow G, Noebe R, Gaydosh D, Garg A. Challenges and progress in the development of high-temperature shape memory alloys based on NiTiX compositions for high-force actuator applications. In: Proceedings of the international conference on shape memory and superelastic technologies, ASM International, Metals Park (OH); 2006.
3. Wadood A, Yamabe-Mitarai Y. TiAu and TiPt high temperature shape memory alloys. In: Proceeding of 2014 11th international Bhurban conference on applied sciences and technology, Pakistan; 2014.
4. He Z, Wang F, Zhou J. Transformation, deformation and microstructure characteristics of $Ru_{50}Ta_{50}$ high temperature shape memory alloy. J Mater Sci Technol. 2006;22–5:634–8.
5. Sathish S, Mallik US, Raju TN. Microstructure and shape memory effect of Cu–Zn–Ni shape memory alloy. J Miner Mater Charact Eng. 2014;2:71–7.
6. Chen J, Li Z, Zhao YY. A high working temperature CuAlMnZr shape memory alloy. J Alloy Compd. 2009;480:481–4.
7. Lelatko J, Morawiec H. High temperature CuAlNb based shape memory alloys. J Phys IV Fr. 2011;11:Pr8-487–92.
8. Yang S, Su Y, Wang C, Liu X. Microstructure and properties of Cu–Al–Fe high-temperature shape memory alloys. Mater Sci Eng B. 2014;185:67–73.
9. Liu Y. Some factors affecting the transformation hysteresis in shape memory alloys. In: Chen HR, editor, chap 13. Nova Science; 2010; p. 361–9.
10. Aydoğdu Y, Kürüm F, Kök M, Yakinci ZD, Aydoğdu A. Thermal properties, microstructure and microhardness of Cu–Al–Co shape memory alloy system. Trans Indian Inst Met. 2014;67–4:595–600.
11. Guilemany JM, Fernandez J. Relationships between structure and hardness developed during the high temperature ageing of a smart Cu-based alloy. J Mater Sci. 1996;31:4981–4.
12. Aydogdu A, Aydogdu Y, Adiguzel O. Long-term ageing behaviour of martensite in shape memory Cu–Al–Ni alloys. J Mater Process Technol. 2004;153–154:164–9.
13. Kürüm F. The production of Cu–Al–Co shape memory alloys and investigation of physical properties. Thesis: M.Sc; 2013 (in Turkish).
14. Bublei IP, Koval YN, Titov PV. Martensitic transformation in alloys of the Cu–Al–Co system. Met Sci Heat Treat. 2008;50: 606–8.
15. Gil FJ, Guilemany JM. Effect of cobalt addition on grain growth kinetics in Cu–Zn–Al shape memory alloys. Intermetallics. 1998;6:445–50.
16. Arruda GJ, Adorno AT, Benedetti AV, Fernandez J, Guilemany JM. Influence of silver additions on the structure and phase transformation of the Cu–13 wt% Al alloy. J Mater Sci. 1997; 32:6299–303.
17. Adorno AT, Silva RAG. Ageing behavior in the Cu–10 wt% Al and Cu–10 wt% Al–4 wt% Ag alloys. J Alloy Compd. 2009; 473:139–44.
18. Wang CP, Liu XJ, Ohnuma I, Kainuma R, Ishida K. Thermodynamic database of the phase diagrams in Cu–Fe base ternary systems. J Phase Equilib Diffus. 2004;25–4:320–8.
19. Wei ZG, Peng HY, Zou WH, Yang DZ. Aging effects in a Cu–12Al–5Ni–2Mn–1Ti shape memory alloy. Metall Mater Trans A. 1997;28A:955–67.
20. Gama JLL, Dantas CC, Quadros NF, Ferreira RAS, Yadava YP. Microstructure-mechanical property relationship to copper alloys with shape memory during thermomechanical treatments. Metall Mater Trans A. 2006;37A:77–87.
21. Ma Y, Jiang C, Deng L, Xu H. Effects of composition and thermal cycle on transformation behaviors, thermal stability and mechanical properties of CuAlAg alloy. J Mater Sci Technol. 2003;19:431–4.
22. Zengin R, Ceylan M. Influence of neutron irradiation on the characteristic of Cu–13 %wt. Al–4 %wt. Ni shape memory alloy. Mater Lett. 2003;58:55–9.
23. Saud SN, Hamzah H, Abubakar T, Zamri M, Tanemura M. Influence of Ti additions on the martensitic phase transformation and mechanical properties of Cu–Al–Ni shape memory alloys. J Therm Anal Calorim. 2014;118:111–22.
24. Yildiz K, Kok M. Study of martensite transformation and microstructural evolution of Cu–Al–Ni–Fe shape memory alloys: effect of heat treatments. J Therm Anal Calorim. 2013;115: 1509–14.

25. Sari U. Influences of 2.5wt% Mn addition on the microstructure and mechanical properties of Cu–Al–Ni shape memory alloys. Int J Miner Metall Mater. 2010;17:192–8.

26. Kayali N, Özgen S, Adigüzel O. The influence of ageing on martensite morphology in shape memory CuZnAl alloys. J Phys IV. 1997;7:C5-317–22.

27. Matlakhova LA, Pereira EC, Matlakhov AN, Monteiro SN, Toledo R. Mechanical behavior and fracture characterization of a monocrystalline Cu–Al–Ni subjected to thermal cycling treatments under load. Mater Charact. 2008;59:1630–7.